Case Studies in Thermal Engineering 55 (2024) 104106

Contents lists available at ScienceDirect

Case Studies in Thermal Engineering

journal homepage: www.elsevier.com/locate/csite

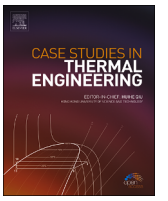

Reaction process and temperature-resistant properties of B/KNO_3/PVDF composites using thermal analysis

Chenyang Li [a, b], Minjie Li [a, b], Haoyu Song [a, b], Xuan Zhan [a, b], Chuanhao Xu [a, b], Baoyun Ye [a, b], Jingyu Wang [a, b], Chongwei An [a, b, *]

[a] School of Environment and Safety Engineering, North University of China, Taiyuan Shanxi, 030051, PR China
[b] Shanxi Engineering Technology Research Centre for Ultrafine Powder, North University of China, Taiyuan Shanxi, 030051, PR China

ARTICLE INFO

Handling Editor: Huihe Qiu

Keywords:
B/KNO_3
Thermal analysis
TG–MS
Reaction process
Temperature resistant properties

ABSTRACT

Using thermal analysis techniques to explore the relation between temperature and physical and chemical changes in materials is crucial for studying the reaction processes of energetic materials. Herein, thermogravimetry–mass spectrometry was used to study the reaction process of B/KNO_3/polyvinylidene fluoride (PVDF) composites. The effects of different PVDF and B contents on the decomposition process, pressure release properties and heat of combustion of the composites were investigated. Furthermore, the thermodynamic and kinetic responses of the composites in a linear integrated state after stimulation at different temperatures were studied. The results show that the addition of PVDF lowered the temperature at which KNO_3 decomposed and released [O], enabling the composite to react at a lower temperature. Although the initial reaction temperature increased with increasing PVDF content, excessive PVDF hindered the heat and mass transfer between particles, thereby deteriorating the pressure release characteristics and heat of combustion of the composite. In addition, the B/KNO_3/PVDF composites were chemically stabilized by heating at 60 ˚C for 90 d or at 150 ˚C for 2 h. This treatment ensured stable combustion and pressure release of the composites. These results provide a reference for studying the reactivity and functional applications of B/KNO_3 composites.

1. Introduction

Energetic materials are characterized by explosive groups or comprise oxidants and fuels that can perform chemical reactions independently, releasing energy. These types of materials are characterized by high energy density and efficient energy release [1,2]. They have become a fundamental component in aerospace [3–5], explosive processing [6,7], detonation [8–10], military pyrotechnics [11–13], and other fields. Studying the reaction process of energetic materials is important for research on their modification and functional application. In recent years, many technologies have emerged for investigating the reaction process of rapid reaction substances [14–18]. Techniques employing Fourier-transform infrared (FTIR) spectroscopy or mass spectrometry (MS) can rapidly detect the reaction products under temperature-jump changes, making them suitable for actual monitoring of reactions. However, these techniques often overlook the changes in the physical and chemical properties of energetic materials with temperature, limiting their effectiveness in studying the reaction process of energetic materials. Thermal analysis is a technique that measures the temperature dependence of the physical properties of substances at a programed temperature [19], and it has been widely used in the field of energetic materials [20–25]. By combining thermal analysis techniques with substance detection methods, researchers can observe the

* Corresponding author. School of Environment and Safety Engineering, North University of China, Taiyuan Shanxi, 030051, PR China.
E-mail address: anchongwei@yeah.net (C. An).

https://doi.org/10.1016/j.csite.2024.104106
Received 9 September 2023; Received in revised form 12 January 2024; Accepted 21 January 2024
Available online 11 February 2024

changes in reaction products with temperature, thereby providing an effective method for studying the reaction process of energetic materials.

Compared with intramolecular energetic materials, intermolecular energetic composites comprising fuels and oxidants exhibit higher energy densities and easier energy release regulation [26–28], making them versatile for various applications. One such component is the B/KNO_3 composite, which is often used as a safe ignition agent in various ignition and fire transmission systems because of its high ignition capacity, high calorific value of combustion, high safety, and satisfactory stability. It is applied in contexts such as explosive sequences [29] and aerospace ignition devices [30,31]. In this composite, B serves as the fuel and KNO_3 functions as the oxidant. The understanding of how fuels and oxidants react and release energy has attracted considerable attention, enabling notable achievements [32,33]. In addition, the introduction of polyvinylidene fluoride (PVDF) in this system allows for the integration of the composite powder using direct ink writing technology [27]. This innovation holds considerable importance for the application of the B/KNO_3 composite in microenergy devices; however, it changes the reaction path of the composite. Although the positive effect of fluorine-containing substances on the removal of the oxide layer of B fuel has been reported [34–38], the influence of PVDF on the oxygen release of the oxidant and the overall reaction system's process has not been studied.

In addition, energetic materials must exhibit long-term thermal stability to maintain stable energy release in practical applications [39]. In other words, these materials must maintain stable reaction thermodynamics and kinetics under different temperature stimuli. This is important for reducing defense budgets, enhancing the safety of energetic materials throughout their life cycle, and addressing complex operational environments. Consequently, the heat-resistant properties of energetic materials have received widespread attention [39–43], particularly for energetic composites comprising active fuels and oxidants, where spontaneous reactions can lead to physical or chemical changes [44,45]. Although the temperature-resistant properties and aging mechanisms of B/KNO_3 have been studied [31,39], these studies have primarily focused on the thermodynamic changes of the composites. The dynamic response of the composites under different heating conditions, particularly the reaction kinetics in the linear integrated state, has not been reported.

In this study, the decomposition processes of the KNO_3 oxidant and KNO_3/PVDF composite were investigated using thermogravimetry (TG)–MS. In addition, the reaction process of the B/KNO_3/PVDF composite was studied. On this basis, the effects of different PVDF and B contents on the reaction process of the composites were analyzed by thermal analysis. The functional relation between the initial reaction temperature of the composite and the PVDF and B contents, as well as the change rule of weight loss, was established. In addition, the thermal decomposition process of the composites under different temperature stimuli was investigated. A high-speed camera and a closed-volume tank were used to demonstrate the dynamic response of the composites to temperature stimuli. These studies not only revealed the influence mechanism of PVDF on the reaction process of B/KNO_3 composites but also examined the thermal stability of the composites under different temperature stimulation conditions. By providing data support for the reactivity study of B/KNO_3 composites, these findings also provide a reference for the functional application of B/KNO_3 composites.

2. Experimental section

2.1. Chemicals

Amorphous boron (B, Nangong Bole Metal Material Co., Ltd., China) was used as the fuel, and potassium nitrate (KNO_3, Chengdu Cologne Chemical Co., Ltd. China) was used as the oxidant. The ultrafine potassium nitrate was prepared by nozzle-assisted simultaneous precipitation (NASP) in the laboratory. Polyvinylidene fluoride (PVDF, Dongguan Shunjie Plastic Technology Co., Ltd. China) was selected as the binder, and N, N-dimethylformamide (DMF, Tianjin Aowei Chemical Reagent Co., Ltd. China) was chosen as the solvent to dissolve the PVDF binder.

2.2. Fabrication and direct ink writing of energetic inks

A certain amount of PVDF was dissolved in DMF to prepare a stable binder solution with a concentration of 1g/20 ml. 93 wt % KNO_3 was placed in the binder solution, and the mixture was homogeneously mixed with the aid of a planetary gravity stirring device (Mianyang Shinuo Technology Co., Ltd. China). The mixture was dried at 60 ˚C for 7 days to obtain a KNO_3/PVDF composite. The binder solution was prepared according to the ratio in Table S1-2, and a certain amount of B and KNO_3 was weighed according to the fuel/oxidant ratios in the table. Then B and KNO_3 were sequentially placed in the prepared PVDF solution and mixed with a planetary gravity stirring device. With the help of direct ink writing (DIW) technology, energetic inks were prepared into energetic sticks [27]. All the energetic sticks were 1 mm × 1 mm × 30 mm.

2.3. Heating treatment of energetic sticks

The energetic sticks were heated using a digital temperature-controlled heating furnace (laboratory-made). The PVDF content in the energetic sticks is 7 wt %, and the ratio of B and KNO_3 is 1:3 (B content is 25 wt %). In a typical experiment, energetic sticks were heated at 60 ˚C for 7 d, 15 d, 30 d, 60 d, and 90 d to verify the long-term thermal stability of energetic composites under 60 ˚C temperature stimulation, which is important for the storage of energetic materials. In addition, the energetic sticks were heated at 150 ˚C, 250 ˚C, and 350 ˚C for 2 h to verify the short-term thermal stability of the energetic composites at higher temperatures, which is very important for the high-temperature environmental adaptability of the energetic composites. In order to avoid the interference of oxygen in the atmospheric environment, all heat treatments were carried out in an argon atmosphere. Before heating, the furnace body was filled with argon (5 L min^{-1} argon flow for 2 min). After starting the heating program, argon was introduced at a flow rate of 20 mL min^{-1}.

2.4. Characterization

After the heating treatments of different heating temperatures and heating times, the microscopic morphology of the energetic sticks was observed by An S4700 scanning electron microscope (SEM, Hitachi, Japan), and the elemental valence states of the different composites were analyzed using an X-ray photoelectron spectroscopy (XPS, Thermo Kalpha, USA) to study the oxidation of the composites at different temperature conditions. A differential scanning calorimeter (DSC, Setaram, France) and a TGA 2 thermogravimetric analyzer (TG, Mettler Toledo, Switzerland) were used to test the thermal decomposition process of different composites and composites treated at different conditions. The test temperature was 50–600 °C and the heating rate was 10 K min^{-1}. The gas products were analyzed by the Thermogravimetric-mass spectrometry method (TG–MS, Rigaku, Japan) to study the reaction process of the composites. The test temperature was 50–800 °C and the heating rate was 10 K min^{-1}. All the tests were carried out in an argon environment. An oxygen bomb calorimeter was used to measure the heat of combustion of the different composites. 1g of the tested composites were weighed, and ignited in an argon atmosphere using the Joule-heated Ni–Cr wire.

2.5. Combustion and pressure output tests

The combustion process of the energetic sticks at different heating temperatures and heating times was observed using an i-SPEED 221 high-speed camera (iX Cameras, UK), and the linear burning rates of the energetic sticks were calculated concerning our previous study [27]. The pressure release characteristics of the composites were tested using a closed-volume tank with a volume of 20 ml. 5 mg of the energetic composite was placed in the center of the tank, and ignited with the Joule-heated Ni–Cr wire of a power supply voltage of 3V.

3. Results and discussion

3.1. Effect of PVDF on the decomposition of KNO_3

Herein, KNO_3 was used as an oxidant, and its decomposition played a major role in the reaction process of the system. The thermal decomposition behavior of KNO_3 was analyzed using thermogravimetric differential thermal analysis (TG–DTG), and the corresponding curves are shown in Fig. 1a. The onset decomposition temperature was approximately 602.05 °C, and the temperature at which

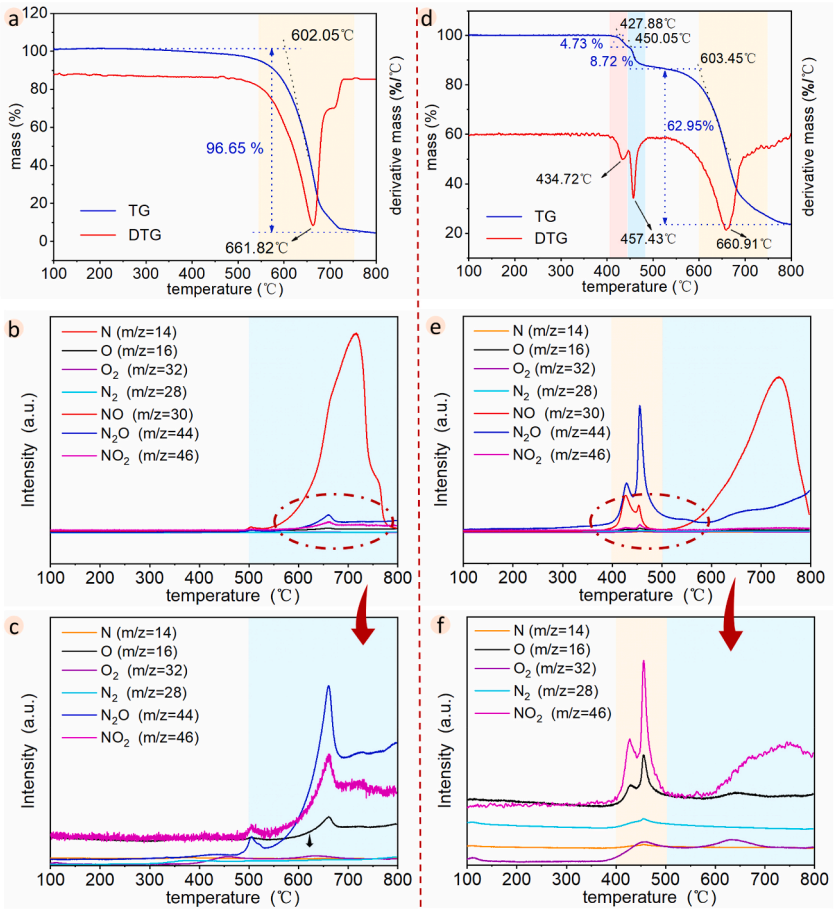

Fig. 1. TG–DTG curve (a) and MS curves (b and c) for KNO_3 and TG–DTG curve (d) and MS curves (e and f) for PVDF/KNO_3.

the reaction reached its maximum rate was approximately 661.82 °C. MS was used to analyze the gaseous reaction products of KNO_3 (Fig. 1b and c). The primary gaseous product of the reaction was NO ($m/z = 30$), which mainly appeared between 500 °C and 800 °C. In addition, the MS curves showed peaks at $m/z = 16$, 32, 44, and 46, corresponding to the release of O, O_2, N_2O, and NO_2, respectively (Fig. 1c). These results indicate that the decomposition reaction of KNO_3 mainly occurs between 500 °C and 800 °C, and the possible reactions are as follows:

$$KNO_3 \rightarrow K^+ + NO + O_2^-$$

$$KNO_3 \rightarrow K^+ + NO_2^- + O$$

$$KNO_3 \rightarrow KO^- + NO + O^+$$

$$2KNO_3 \rightarrow 2KO^- + N_2O^- + 3O^+$$

After the addition of 7 wt% PVDF, the decomposition reaction of the composite changed from one to three stages (Fig. 1d). The onset temperature of the first reaction stage was 427.88 °C, which is consistent with the decomposition temperature of PVDF (Fig. S1). Therefore, the reaction in the first stage may correspond to the decomposition of PVDF. The onset temperature of the second reaction stage was 450.05 °C, and the temperature at which the reaction reached the maximum reaction rate was approximately 457.43 °C. This result indicates that the addition of PVDF facilitated the decomposition of KNO_3 at a lower temperature. The third reaction stage started at 603.45 °C, and the temperature at which the reaction reached its maximum rate was approximately 660.91 °C, which was consistent with the decomposition of KNO_3. According to the MS curves (Fig. 1e), the main gaseous products of the decomposition of KNO_3 with the addition of PVDF were N_2O ($m/z = 44$) and NO ($m/z = 30$). N_2O was mainly released at 400°C-500 °C, corresponding to the second stage of the reaction. Conversely, NO was released at 400°C-500 °C and 500°C-800 °C, corresponding to the second and third stages of the reaction. In addition, peaks at $m/z = 14$, 16, 28, 32, and 46 were observed between 400 °C and 500 °C (Fig. 1f), representing the release of N, O, N_2, O_2, and NO_2, respectively. Peaks corresponding to O, O_2, and NO_2 were also observed between 500 °C and 800 °C. Therefore, the addition of PVDF advanced the decomposition temperature of KNO_3 from 500°C-800 °C to 400°C-500 °C, with N_2O becoming the dominant gaseous product in this temperature range. Notably, N_2O decomposes at high temperatures to produce oxidizing gas. Possible reactions may include the following:

$$N_2O \rightarrow N_2^- + O^+$$

$$N_2O \rightarrow NO^- + N^+$$

$$2N_2O \rightarrow 2N_2 + O_2$$

The results show that the decomposition products of KNO_3 are dominated by NO. However, with the addition of PVDF, the decomposition pathway of KNO_3 was changed, leading to an advancement in the decomposition temperature and the generation of NO and N_2O as the main products. Consequently, KNO_3, as an oxidizing agent, does not directly decompose to produce a large amount of oxygen to participate in the reaction. Instead, it decomposes to produce oxidizing species [O] that actively participate in the reaction of the composite. These oxidizing species may include oxide ions, oxygen ions, oxidizing fragments, and a small amount of gaseous oxygen.

3.2. Effect of PVDF on the reaction process of B/KNO_3 composites

The differential scanning calorimetry (DSC) curves of the energetic composites are shown in Fig. 2a. Two endothermic peaks appeared at approximately 139.2 °C and 332.76 °C, corresponding to the transcrystallization and melting of KNO_3, respectively. This is consistent with the DSC curve of KNO_3 (Fig. S2). However, B/KNO_3 exhibited single-stage decomposition with a reaction peak temperature of 549.1 °C, as evidenced by the TG–DTG curve (Fig. S3). The MS analysis results (Fig. 2b) revealed the presence of a single NO peak with a peak temperature of 551.38 °C, which is consistent with the reaction stage observed in the DSC and TG curves. However, the reaction temperature of the composite was much lower than that of KNO_3, and the reaction occurred before the release of the oxidizing gasses. Therefore, the reaction of B/KNO_3 can be better explained by a condensed-phase reaction. As shown in Fig. 2c, KNO_3 melts at 332.76 °C and wraps the B particles, and the melting point of B_2O_3 is approximately 450 °C. Therefore, the [O] species in the molten KNO_3 diffuses through the molten layer to the B nucleus, where it undergoes a slow redox reaction with B. The heat generated by this reaction accumulates until the system reaches its ignition temperature (538.76 °C).

After the addition of 7 wt% PVDF, the peak temperature of the main reaction appeared at 489.3 °C, which was 59.8 °C lower than that of the B/KNO_3 composite. Furthermore, compared with the B/KNO_3 composite, distinct exothermic peaks appeared in the range of 420 °C-470 °C, indicating an earlier occurrence of the reaction. This change was caused by the early decomposition of KNO_3 under the action of PVDF, because the DSC curve of PVDF/KNO_3 composite also showed exothermic peaks in this temperature range (Fig. S4). The PVDF/KNO_3 composite decomposed at 427.88°C-456.44 °C (Fig. 2d), where the generated [O] species ignited with B in advance through the molten layer. Therefore, the MS analysis of the B/KNO_3/PVDF composite exhibited a strong NO release peak in the range of 400°C-500 °C (Fig. 2b). In addition, a small NO release peak appeared at 589.35 °C, which was also observed in the MS curve of the B/KNO_3 composite. This phenomenon can be attributed to the decomposition of excess KNO_3. Notably, compared with the decomposition of KNO_3 and PVDF/KNO_3 composites, this temperature was increased by approximately 46 °C because of the influence of the exothermic reaction in the system.

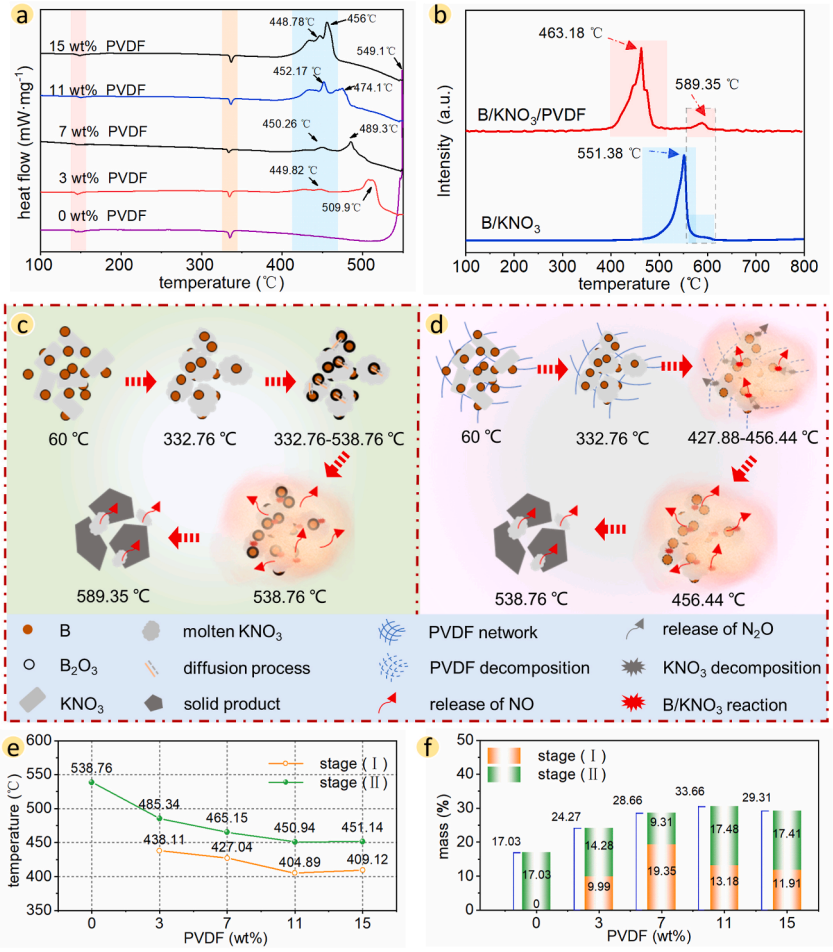

Fig. 2. DSC curves of composites with different PVDF contents (a), MS curves of B/KNO_3 and B/KNO_3/PVDF at m/z = 30 (b), and the reaction process of the two composites (c and d). The initial reaction temperature curve (e) and the weight loss at different reaction stages (f) of composites with different PVDF contents.

Moreover, as the PVDF content increased from 3 to 15 wt%, the peak temperature of the main reaction decreased from 509.9 ˚C to 456 ˚C. In addition, the TG–DTG curves of energetic composites with different PVDF contents (Fig. S5) exhibited two stages of the decomposition reaction. Based on the tangent method, the onset reaction temperature and weight loss of all curves at different reaction stages were determined (Fig. 2e and f). Compared with the B/KNO_3 composite, the initial reaction temperature of the main reaction of the composite decreased from 538.76 ˚C to 450.94 ˚C after the addition of PVDF. With an increase in the PVDF content from 3 to 11 wt%, the initial reaction temperature of the first stage of the reaction decreased from 438.11 ˚C to 404.89 ˚C, and the weight loss increased from 17.03% to 33.66%, indicating a more complete redox reaction. On the one hand, the addition of more PVDF results in the production of more oxidizing substance [O] in the temperature range of 400˚C-500 ˚C, facilitating an easier ignition reaction for B. On the other hand, the decomposition of PVDF, which contains a high content of F and H, can produce a large amount of HF gas or F–C fragments (Fig. S6). These substances can react with the high boiling point and low melting point oxide layer (B_2O_3) on the outer layer of B, thereby eliminating the limitation of the redox reaction due to the inert oxide layer and condensed-phase products [46–48]. However, note that a very high PVDF content hinders the heat and mass transfer of the composite. As the PVDF content continues to increase, the initial reaction temperature of the composite no longer increases, and the weight loss decreases.

3.3. Effect of B content on the reaction process of the composites

The fuel and oxidant contents in the system also affect the reaction process of the composite. When the B content was 10 wt% (Fig. 3a), the DSC curve of the composites exhibited multiple peaks. The first three peaks represent the decomposition of PVDF/KNO_3 and the exothermic reaction of B with the oxidizing substance [O]. The last two peaks represent the main reaction of B with KNO_3. However, at this time, the system was in a fuel-poor state, indicating that there was not enough fuel to participate in the redox reaction. In addition, some of the heat generated during the reaction was used to decompose excess KNO_3. Therefore, the exothermic peaks of the reaction were more disorganized because of the influence of the endothermic reaction. The TG–DTG curve (Fig. S7a) exhibited three reaction stages. Furthermore, based on the MS curve (Fig. 4a), when the B content was 10 wt%, the curve exhibited three stages of NO release. The first and second stages corresponded to the reaction of the two stages of the composite, and the NO release in the third

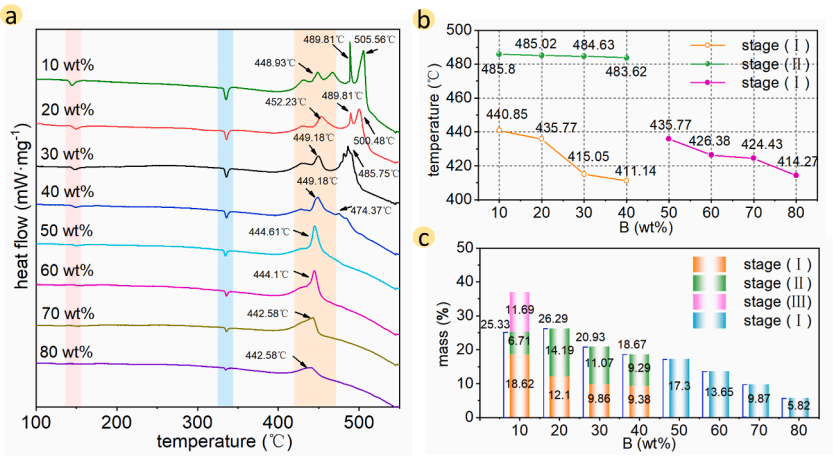

Fig. 3. DSC curves (a), initial reaction temperature curves (b), and weight loss image at different reaction stages (c) of composites with different B contents.

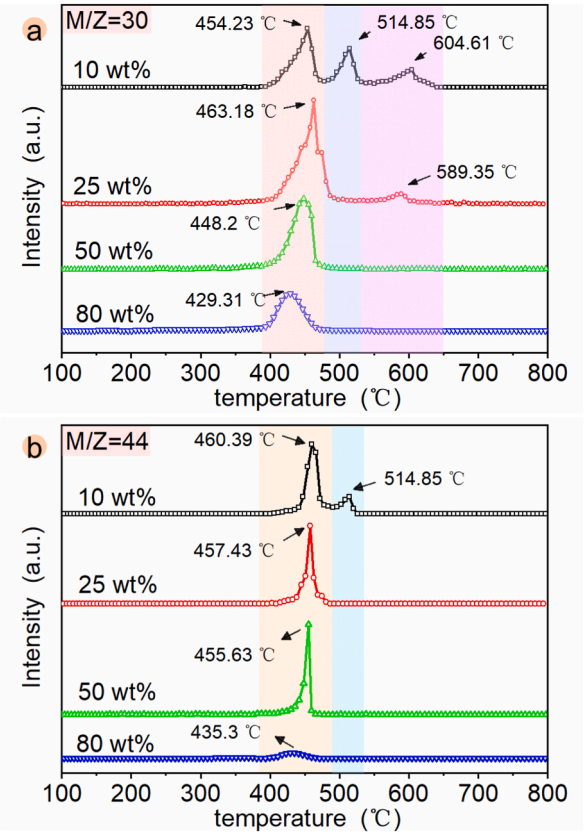

Fig. 4. NO (a) and N_2O (b) release curves of composites with different B contents.

stage represented the decomposition of excess KNO_3. As the B content increased up to 40 wt%, the system became slightly fuel-rich. The excess fuel compensated for the proportion of the inert oxide shell in the system and the fuel loss caused by the condensed-phase reaction, resulting in an almost complete reaction. The last two exothermic peaks of the DSC curve merged, and the reaction transformed from three to two stages (Fig. S7 b–d). As the B content continued to increase to 80 wt%, the DSC curve exhibited only one reaction exothermic peak, and the TG–DTG curves exhibited a single-stage reaction (Fig. S7 e–h). The MS curves (Fig. 4a) exhibited a gradual change toward single-stage NO release. This change occurred because the system had entered the fuel-rich stage with insufficient oxidant to support a complete reaction. This is evidenced by the XRD results of the condensed phase products (Fig. S8). The peak shape gradually shifted to a bulging peak with increasing B content, as the amount of unreacted amorphous B in the product increased. In addition, the MS curves of the composites with different B contents showed a peak of N_2O between 400 °C and 500 °C (Fig.

4b), indicating that the addition of PVDF promoted the early decomposition of KNO_3, thereby allowing the composites to proceed at a lower temperature. This is consistent with the results presented in the previous section.

Note that the mass fractions of B and KNO_3 here do not consider the PVDF content, as the PVDF content remained constant in all formulations (7 wt%). As the B content increased from 10 to 80 wt%, the intensity of the endothermic peaks representing the crystallization and melting of KNO_3 at approximately 139.2 °C and 332.7 °C decreased gradually because of the decreasing KNO_3 content. The exothermic peak temperature of the first stage of the reaction decreased from 452.23 °C to 442.58 °C with increasing B content. According to the TG–DTG curve, the initial reaction temperature curve and weight loss diagram of the different composites were plotted (Fig. 3b and c). As the B content increased from 10 to 40 wt%, the initial reaction temperatures of the first and second stages of the reaction decreased from 485.8 °C to 440.85 °C–483.62 °C and 411.14 °C, respectively. When the B content increased from 50 to 80 wt%, the initial reaction temperature decreased from 435.77 °C to 414.27 °C. Although the initial reaction temperature increased with increasing B content, the completeness of the reaction was reduced, as evidenced by a decrease in the weight loss of the system. This reduction occurred because the oxidant was insufficient to fully react with the fuel.

3.4. Pressure output characteristics of the composites

The pressure output characteristic of the composites is an essential property for assessing the reactivity of energetic materials. Based on the pressure–time curves of the different composites (Fig. 5a and c), the pressurization rate is plotted as a function of the PVDF and B contents in Fig. 5b and d. The maximum pressure and pressurization rate of the composites exhibited an increasing and then decreasing trend with increasing PVDF content, reaching their maximum value at 3 wt% PVDF content (5.98 MPa, 372.19 MPa s^{-1}). However, when the PVDF content continued to increase to 15 wt%, the maximum pressure of the composites decreased to 2.21 MPa, and the pressurization rate decreased to 78.09 MPa s^{-1}, which were only 39.25% and 29.08% of the composite without PVDF, respectively. The addition of a certain amount of PVDF facilitated the decomposition of KNO_3, and the HF and fluorocarbon fragments produced from the PVDF decomposition eliminated the limitations of the inert oxide layer. However, the excessive addition of an inert binder hindered the contact between the fuel and oxidant, thereby reducing the heat and mass transfer rates and lowering the pressure output characteristics of the composites.

The fuel content in the reaction system similarly affects the pressure release characteristics (Fig. 5c and d) because of the different reaction rates and completeness. Previous studies have shown that a slightly fuel-rich environment is advantageous for the reaction of energetic composites because it compensates for the percentage of inert oxide layer in the composites and the loss of unreacted fuel in the condensed phase [27]. The highest weight loss was observed at a B content of 10 wt% (Fig. 3c) because the decomposition of the excess oxidant produced more gas. However, higher gas production does not necessarily translate to higher pressure release characteristics, particularly in terms of the pressurization rate, because pressure release capacity is also related to the reaction time. At this point, the content of B (10 wt%) was insufficient, resulting in lower reaction energy and rate, leading to lower maximum pressure and pressurization rate of the composite. The redox reaction was the most complete when the B content was between 20% and 30%. At this time, the pressure–time curve exhibited the largest peak value with a sharp shape, indicating a higher pressure release and a shorter reaction time, resulting in the highest pressurization rate. As the B content continued to increase, the amount of oxidant in the reaction system became insufficient to completely oxidize all the fuels, leading to reduced reaction efficiency and heat release. The

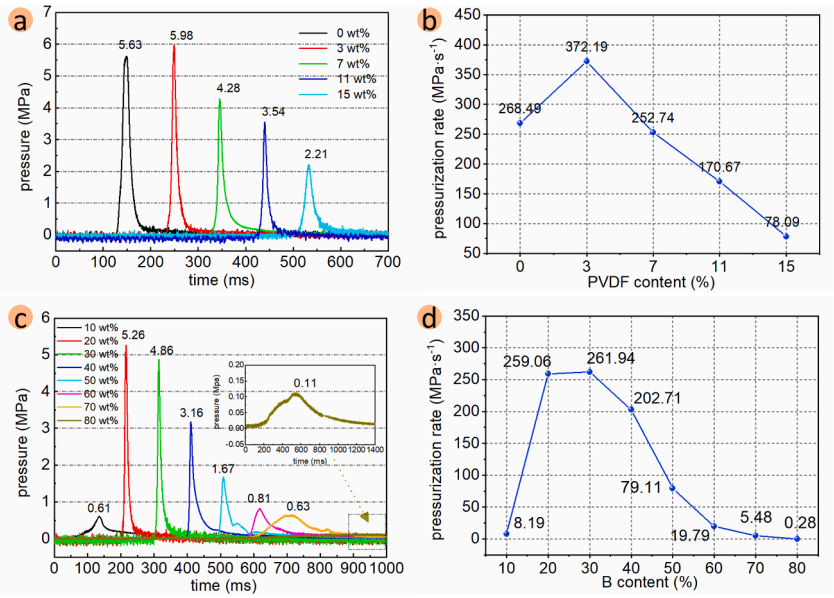

Fig. 5. Pressure release test results for different composites. Pressure–time curves (a) and pressurization rate curve (b) of composites with different PVDF contents when the content of B is 25 wt%. Pressure–time curves (c) and pressurization rate curve (d) of composites with different B contents when the content of PVDF is 7 wt%.

peak shape of the pressure–time curve became gentler, the peak pressure decreased, and the reaction time increased, resulting in a decrease in the pressurization rate. When the B content was 80%, the peak pressure was 0.11 MPa and the pressurization rate decreased to 0.28 MPa s^{-1}. Therefore, the pressure release characteristics of energetic composites can be controlled by adjusting the binder content and fuel/oxidant ratio in the reaction system.

3.5. Heat of combustion of composites

Testing the heat of combustion of composites is important for studying heat release during combustion. When the B to KNO_3 ratio is 1:3, the heat of combustion gradually decreases as the PVDF content increases from 0 to 15 wt% (Fig. 6a). This indicates that the addition of excess PVDF affects the heat release of the composite. Several possible reasons account for this observation: 1. The fuel in the composite system decreases with increasing PVDF. 2. Excessive PVDF and its solid decomposition products hinder heat and mass transfer between the fuel and oxidant. 3. The decomposition of PVDF requires heat absorption. Note that the magnitude of the reduction in the heat of combustion of the composite increases with higher PVDF content, particularly when the PVDF content is > 7 wt%. When the PVDF content is constant (taking a PVDF content of 7 wt% as an example), the heat of combustion changes with the change in the B content. The heat of combustion shows a trend of increase–stability–decrease (Fig. 6b). When the B content is between 20 wt % and 30 wt %, the heat of combustion reaches the maximum. At this point, the system is slightly fuel-rich and the redox reaction of the composite is complete. Neither an excess of fuel nor an excess of oxidizer promotes the exothermic nature of the reaction.

3.6. Effect of heating stimulus on the decomposition process of composites

After heating the composites at 60 °C for 15–90 d, the TG test was performed. The results showed that the TG curves of all the composites closely matched those of the composites heated at 60 °C for 7 d (Fig. 7a), with weight loss rates of approximately 28%. This implies that the B/KNO_3/PVDF composites exhibited remarkable chemical composition stability over an extended period at 60 °C, which is of great importance for the storage of energetic composites. Similarly, the composite demonstrated good stability after

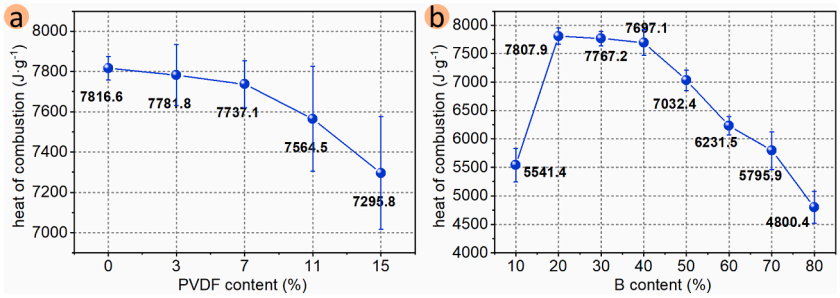

Fig. 6. Heat of combustion of composites with different PVDF contents (a) and different B contents (b).

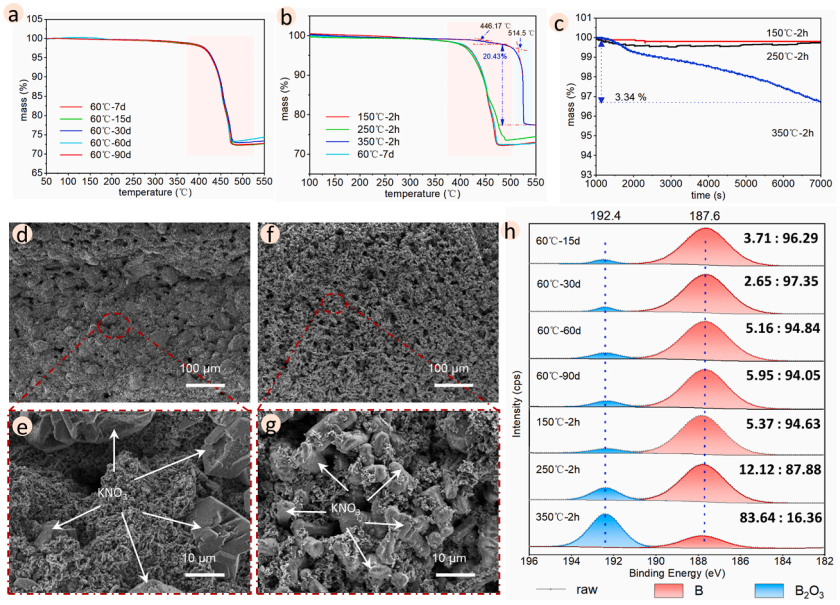

Fig. 7. TG results of the composites at different heating temperatures and heating times (a–c); SEM images of samples heated at 350 °C for 2 h (d and e) and 60 °C for 7 d (f and g). XPS results of the composites at different heating temperatures and heating times (h).

heating at 150 °C for 2 h (Fig. 7b). The weight loss rate decreased after heating at 250 °C for 2 h. This result could be attributed to the slow redox reaction occurring in the composite at this temperature. However, when heated at 350 °C for 2 h, the reaction process of the energetic composites changed. The initial temperature of the first stage reaction was delayed from 427.04 °C to 446.17 °C, the initial temperature of the second stage reaction was delayed from 465.15 °C to 514.5 °C, and the weight loss rate was reduced from 28.66% to 20.43%. This indicates that the reactivity of the energetic composite was reduced because the reaction could only occur at higher temperatures.

On the one hand, the melting point of KNO_3 particles is approximately 335 °C (Fig. S2), and the solidification of molten KNO_3 after the temperature decrease causes an increase in the particle size of KNO_3. After heating at 350 °C for 2 h (Fig. 7d and e), the particle size of KNO_3 was considerably larger than that of ultrafine potassium nitrate particles (Fig. 7f and g). This notable increase in particle size reduced the contact area between the fuel and oxidant and subsequently decreased the reaction efficiency of the composites. TG analysis was performed to measure the weight loss of the original composite (dried at 60 °C for 7 d) at 150 °C, 250 °C, and 350 °C for 2 h. The weight loss increased slowly when the composite was heated to 350 °C. Molten KNO_3 encapsulates the B particles and reacts with B in the condensed phase, thereby increasing the thickness of the inert oxide layer on the outside of B and reducing the activity and reactivity of B particles. This observation is supported by an X-ray photoelectron spectroscopy (XPS) diagram of the composite. When heated at 350 °C for 2 h (Fig. 7h), the content of B_2O_3 on the surface of the composite increased, indicating a thickening of the outer layer of the B_2O_3 oxide shell. The ignition process of B is influenced by the bidirectional diffusion of fuel/oxidant [49,50], and the increase in the inert B_2O_3 oxide layer with a low melting point and high boiling point hinders the heat and mass transfer of the redox reaction, thereby reducing the reaction efficiency of the composite. In addition, the ratio of B_2O_3 to B on the surface of the composite did not substantially change after heating at 60 °C for 15–90 d or at 150 °C for 2 h, indicating that the composite maintained good chemical stability at this temperature. However, after heating at 250 °C for 2 h, the content of B_2O_3 on the surface of the composite slightly increased, which affected the reactivity of the composite to a certain extent. These results are consistent with the TG test results.

3.7. Effect of heating stimulus on the reactivity of composites

The ignition and combustion experiments were performed after various heating treatments. The flame propagation trajectories were observed, and the linear burning rates of the different energetic sticks were calculated. Compared with the combustion process of the energetic sticks heated at 60 °C for 15 d (Fig. 8a), the flame morphology of the energetic sticks heated at 60 °C for 30, 60, and 90 d (Figs. S9a–c) did not substantially change. Similarly, the flame propagation process and shape of the energetic stick heated at 150 °C and 250 °C for 2 h (Figs. S9d and e) remained relatively stable, with all flame fronts exhibiting stable linear propagation. However, when heated at 350 °C for 2 h (Fig. 8b), the flame area was considerably reduced, and no scorching particles were ejected outward. During the combustion process of the energetic stick (Fig. 8c and d), the fuel and oxidant in the reaction zone undergo a redox reaction, releasing a large amount of gas and generating pressure. This pressure propagates in the porous stick, providing a driving force for the forward propagation of the flame. Simultaneously, the pressure diffuses outside the stick, causing the solid products to splash in the direction opposite to flame propagation to form a flame zone. Therefore, the reaction kinetics of the energetic sticks are closely related to the reaction pressure. When the heating temperature reached 350 °C, the oxide layer around B became thicker, and the pure B content decreased (Fig. 8e). In addition, the inert oxide layer hindered heat transfer and the diffusion of fuel/oxidant, thereby reducing the accumulation and propagation of reaction pressure. Consequently, this reduced the reaction kinetic characteristics of the sticks.

The linear burning rates of the energetic sticks were calculated, and the results are presented in Fig. 8f and g. When the energetic sticks were heated at 60 °C for 15, 30, 60, and 90 d, the burning rates were 59.55, 59.97, 60.42, and 59.55 mm s^{-1}, respectively. The standard deviations (SD) of all experiments were within 3 mm s^{-1}, indicating minimal differences in reaction kinetics and excellent chemical stability. The linear burning rates of the energetic sticks slightly increased to 70.93 and 75.39 mm s^{-1} when heated at 150 °C and 250 °C for 2 h. This can be attributed to the boiling point of dimethylformamide (DMF), which is approximately 153 °C. The heating process resulted in a more complete volatilization of DMF from the energetic sticks. Furthermore, when heated to a temperature of 250 °C, PVDF melted, and after cooling, the melted PVDF solidified, causing the internal pore structure of the stick to change. As a result, the SD of the linear burning rate was higher. However, when the sticks were heated at 350 °C for 2 h, the linear burning rate substantially decreased to approximately 12.56 mm s^{-1}. Similarly, the pressure output characteristics of the energetic composites exhibited similar trends (Fig. 8h and i). The peak pressures of the composites did not considerably change when heated at 60 °C for $<$90 d, which were all approximately 4.3 MPa. When heated at 350 °C for 2 h, the pressure release decayed because of the slow redox reaction of the composites in the molten state, resulting in a reduction in the peak pressure to approximately 1.5 MPa.

4. Conclusion

Herein, the reaction process of B/KNO_3/PVDF energetic composites with different PVDF and B contents was studied using TG–MS. Furthermore, the pressure output characteristics of the different composites were studied. The effects of different temperature treatments on the decomposition and reaction properties of the energetic sticks were also studied. The results showed that a condensed-phase reaction occurred between B/KNO_3 because the reaction was performed before the decomposition of the oxidant, and the oxidant had no obvious oxidizing gas release. The addition of PVDF changed the decomposition path of KNO_3, causing it to decompose between 400 °C and 500 °C and releasing more N_2O gas during this stage. This led to the oxidant decomposing at a lower temperature and producing the oxidizing substance [O], which reacted with B in advance. Therefore, the reaction temperature of the B/KNO_3/PVDF composite was approximately 100 °C earlier than that of the B/KNO_3 composite. By increasing the PVDF content from

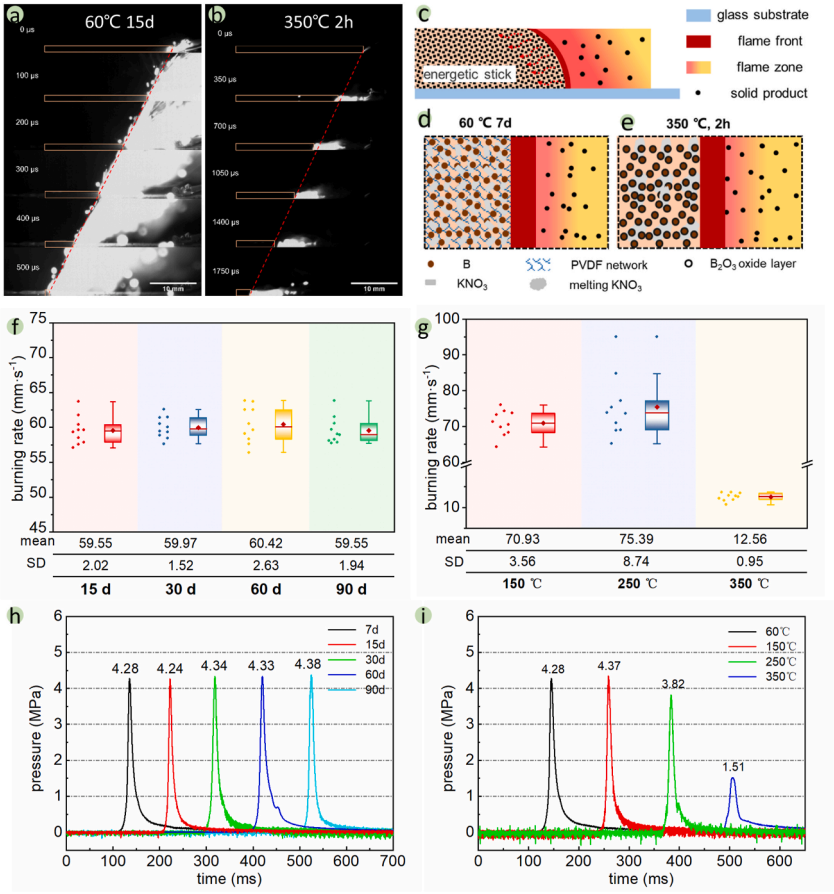

Fig. 8. Combustion snapshots of energetic sticks heated at 60 ˚C for 15 d (a) and 350 ˚C for 3 h (b); schematics of the reaction processes of the energetic sticks under different heating conditions (c–e); burning rate distribution images of energetic sticks heated at 60 ˚C for long periods (f) and at high temperature for 2 h (g); and the pressure–time curves of energetic sticks heated at 60 ˚C for long periods (h) and at high temperature for 2 h (i).

3 to 11 wt%, the initial reaction temperature of the system decreased from 438.11 ˚C to 404.89 ˚C. However, the addition of excessive PVDF hindered the reaction because the inert material impeded heat and mass transfer between particles. Therefore, when the PVDF content exceeded 11 wt%, the initial reaction temperature of the composite no longer advanced, and the weight loss was reduced. In addition, according to the pressure–time curves, with increasing PVDF content, the maximum pressure and pressurization rate of the composite decreased because the obstruction of heat and mass transfer led to a decrease in the reaction characteristics of the system. Although the initial temperature of the reaction slightly advanced with increasing B content, an excessive amount of fuel or oxidant was unfavorable for the complete reaction of the composites, resulting in poor reactivity. The pressure–time curves of composites with different B contents showed the highest pressure release and pressurization rate when the B content was between 20% and 30% (slightly fuel-rich). The thermal decomposition, combustion, and pressure output characteristics of the energetic sticks exhibited minimal changes within 90 d of heating at 60 ˚C and 2 h of heating at 150 ˚C, indicating good thermal stability of the energetic sticks under these conditions. However, when heated at 350 ˚C for 2 h, KNO_3 in the energetic stick melted and underwent a slow redox reaction with B, increasing the B_2O_3 content in the composite and decreasing the active B content. Therefore, the pressure output characteristics and combustion performance were reduced. This study demonstrates the reaction path of the B/KNO_3/PVDF composite, reveals the influence of the composition and ratio on the reaction characteristics, and provides a reference for studying the reactivity of B/KNO_3. In addition, the temperature-resistant characteristics of B/KNO_3 composites under temperature stimuli were studied, providing a reference for the long-term storage of energetic composites and their adaptability to high-temperature environments.

Funding

This work was supported by the National Natural Science Foundation of China (No. 22275170) and the National Natural Science Foundation of China (No. 22105184).

CRediT authorship contribution statement

Chenyang Li: Data curation, Writing – original draft. **Minjie Li:** Investigation. **Haoyu Song:** Investigation. **Xuan Zhan:** Investigation. **Chuanhao Xu:** Funding acquisition, Methodology. **Baoyun Ye:** Validation. **Jingyu Wang:** Supervision, Validation. **Chongwei An:** Funding acquisition, Writing – review & editing.

Declaration of competing interest

The authors declare that they have no known competing financial interests or personal relationships that could have appeared to influence the work reported in this paper.

Data availability

No data was used for the research described in the article.

Acknowledgments

The authors thank the Institute of Coal Chemistry, Chinese Academy of Sciences for the support of SEM–EDS test. The authors also thank Shiyanjia Lab (http://www.shiyanjia. com) for the support of language editing service.

Appendix A. Supplementary data

Supplementary data to this article can be found online at https://doi.org/10.1016/j.csite.2024.104106.

References

[1] J. Liu, L. Liu, X. Liu, Development of high-energy-density materials, Sci. China Technol. Sci. 63 (2020) 195–213.
[2] W. Zhang, J. Zhang, M. Deng, X. Qi, F. Nie, Q. Zhang, A promising high-energy density material, Nat. Commun. 8 (2017) 181.
[3] M. Li, R. Hu, M. Xu, Q. Wang, W. Yang, Burning characteristics of high density foamed GAP/CL-20 propellants, Def. Technol. 18 (2022) 1914–1921.
[4] S. Chaturvedi, P.N. Dave, Solid propellants: AP/HTPB composite propellants, Arab. J. Chem. 12 (2019) 2061–2068.
[5] Y. Wang, J. Wen, J. Yang, G. Zhang, N. Wang, Y. Wu, Investigations on the thermal response of a solid rocket motor with complex charge structure using CL-20/GAP propellant, Case Stud. Therm. Eng. 37 (2022) 102257.
[6] E.V. Kuz'min, V.I. Lysak, S.V. Kuz'min, M.P. Korolev, Influence of structure formation and properties of bimetal produced by ultrasound-assisted explosive welding 71 (2021) 734–742.
[7] M.J. Langenderfer, Y. Zhou, J. Watts, W.G. Fahrenholtz, C.E. Johnson, Detonation synthesis of nanoscale silicon carbide from elemental silicon, Ceram. Int. 48 (2022) 4456–4463.
[8] L. Zhang, F. Zhang, Y. Wang, R. Han, J. Chen, R. Zhang, E. Chu, In-situ preparation of copper azide by direct ink writing, Mater. Lett. 238 (2019) 130–133.
[9] C. Li, S. Kong, D. Liao, C. An, B. Ye, J. Wang, Fabrication and characterization of mussel-inspired layer-by-layer assembled CL-20-based energetic films via micro-jet printing, Def. Technol 18 (2022) 1748–1759.
[10] B. Ye, C. Song, H. Huang, Q. Li, C. An, J. Wang, Direct ink writing of 3D-Honeycombed CL-20 structures with low critical size, Def. Technol 16 (2020) 588–595.
[11] S. Zhao, Z. Han, M. Li, H. Liu, R.A. Mensah, O. Das, L. Jiang, Insights into thermochemistry, kinetics, and pyrolysis behavior of green gas generator 5-aminotetrazole by experiment and theoretical methods, Case Stud. Therm. Eng. 49 (2023) 103217.
[12] M.C. Rehwoldt, H. Wang, D.J. Kline, T. Wu, N. Eckman, P. Wang, N.R. Agrawal, M.R. Zachariah, Ignition and combustion analysis of direct write fabricated aluminum/metal oxide/PVDF films, Combust. Flame 211 (2020) 260–269.
[13] J.C. Poret, A.P. Shaw, C.M. Csernica, K.D. Oyler, J.A. Vanatta, G. Chen, Versatile boron carbide-based energetic time delay compositions, ACS Sustainable Chem. Eng. 1 (2013) 1333–1338.
[14] L. Zhou, N. Piekiel, S. Chowdhury, M.R. Zachariah, T-Jump/time-of-flight Mass Spectrometry for Time-Resolved Analysis of Energetic Materials, vol. 23, 2009, pp. 194–202.
[15] T.S. Ward, M.A. Trunov, M. Schoenitz, E.L. Dreizin, Experimental methodology and heat transfer model for identification of ignition kinetics of powdered fuels, Int. J. Heat Mass Tran. 49 (2006) 4943–4954.
[16] Y. Jiang, S. Deng, S. Hong, S. Tiwari, H. Chen, K. Nomura, R.K. Kalia, A. Nakano, P. Vashishta, M.R. Zachariah, X. Zheng, Synergistically chemical and thermal coupling between graphene oxide and graphene fluoride for enhancing aluminum combustion, ACS Appl. Mater. Interfaces 12 (2020) 7451–7458.
[17] F. Xu, B. Hirt, P. Biswas, D.J. Kline, Y. Yang, H. Wang, A. Sehirlioglu, M.R. Zachariah, Superior reactivity of ferroelectric Bi_2WO_6/aluminum metastable intermolecular composite, Chem. Eng. Sci. 247 (2022) 116898.
[18] F. Xu, P. Biswas, P. Ghildiyal, M.R. Zachariah, Inducing oxygen vacancies to modulate ignition threshold of nanothermites, Energy Fuels 36 (2022) 5878–5884.
[19] M.J. Richardson, Thermal analysis, in: G. Allen, J.C. Bevington (Eds.), Comprehensive Polymer Science and Supplements, vol. 1, Elsevier Ltd, 1996, pp. 867–901.
[20] M. Yang, J.J. Yoh, C. Tang, Z. Huang, Effect of tungsten size on thermal analysis and mechanism of lithium perchlorate-based electrically controlled solid propellant, Case Stud. Therm. Eng. 47 (2023) 103135.
[21] D. Zheng, T. Huang, B. Xu, X. Zhou, Y. Mao, L. Zhong, B. Gao, D. Wang, 3D printing of n-Al/Polytetrafluoroethylene-Based energy composites with excellent combustion stability, Adv. Eng. Mater. 23 (2021) 2001252.
[22] M.A. Hobosyan, K.G. Kirakosyan, S.L. Kharatyan, K.S. Martirosyan, PTFE–Al2O3 reactive interaction at high heating rates, J. Therm. Anal. Calorim. 119 (2015) 245–251.
[23] M. Li, C. Li, Y. Song, C. Li, W. Cheng, C. Xu, N. Yun, C. An, Thermal decomposition reaction mechanism and combustion performance of AlH_3/AP energetic composite 38 (2022) 102317.
[24] A. Eslami, S.G. Hosseini, S.M. Pourmortazavi, Thermoanalytical investigation on some boron–fuelled binary pyrotechnic systems, Fuel 87 (2008) 3339–3343.
[25] B. Roduit, C. Borgeat, B. Berger, P. Folly, B. Alonso, J.N. Aebischer, F. Stoessel, Advanced kinetic tools for the evaluation of decomposition reactions: determination of thermal stability of energetic materials, J. Therm. Anal. Calorim. 80 (2005) 229–236.
[26] W. He, P. Liu, G. He, M. Gozin, Q. Yan, Highly reactive metastable intermixed composites (MICs): preparation and characterization, Adv. Mater. 30 (2018) 1706293.
[27] C. Li, H. Song, C. Xu, C. Li, J. Jing, B. Ye, J. Wang, C. An, Reactivity regulation of B/KNO_3/PVDF energetic sticks prepared by direct ink writing, Chem. Eng. J. 450 (2022) 138376.
[28] K.T. Sullivan, J.D. Kuntz, A.E. Gash, Electrophoretic deposition and mechanistic studies of nano-Al/CuO thermites, J. Appl. Phys. 112 (2012) 024316.
[29] Military Standard, Munition Rocket and Missile Motor Ignition System Design Safety Criteria for, MIL-STD-1901, 1992.
[30] J. Asakawa, H. Koizumi, S. Kojima, et al., Total impulse increase of a micro-solid rocket using a stack of B/KNO_3 pellets, Trans. JSASS Aerospace Tech. Jpn. 14 (2016) 53–59.

[31] C. Li, N. Yan, Y. Ye, et al., Thermal analysis and stability of boron/potassium nitrate pyrotechnic composition at 180°C, Appl. Sci. 9 (2019) 3630.
[32] W. Zhang, R. Shen, L. Wu, Y. Chen, Y. Ye, Y. Hu, P. Zhu, Reaction mechanism of B/KNO_3 under laser irradiation, Adv. Mater. Res. 554–556 (2012) 457–460.
[33] J. Sivan, Y. Haas, Spectroscopic characterization of B/KNO_3 diode-laser induced combustion, J. Phys. Chem. A 117 (2013) 11808–11814.
[34] F. Xiao, C. Chen, Z. Chen, J. Hu, In situ precise construction of surface-activated boron powders: a new strategy to synergistically improve the interface properties and enhance combustion performance of boron, Fuel 351 (2023) 128995.
[35] L. Cheng, C. Huang, Y. Yang, Y. Li, Y. Meng, Y. Li, H. Chen, D. Song, R. Artiaga, Preparation and combustion performance of B/PVDF/Al composite microspheres, Propellants, Explos. Pyrotech. 45 (2020) 657–664.
[36] K.L. Chintersingh, M. Schoenitz, E.L. Dreizin, Oxidation kinetics and combustion of boron particles with modified surface, Combust. Flame 173 (2016) 288–295.
[37] G. Young, C.A. Stoltz, D.H. Mayo, C.W. Roberts, C.L. Milby, Combustion behavior of solid fuels based on PTFE/boron mixtures, Combust. Sci. Technol. 185 (2013) 1261–1280.
[38] S.K. Valluri, M. Schoenitz, E. Dreizin, Bismuth fluoride-coated boron powders as enhanced fuels, Combust. Flame 221 (2020) 1–10.
[39] J. Lee, T. Kim, S.U. Ryu, K. Choi, G.H. Ahn, J.G. Paik, B. Ryu, T. Park, Y.S. Won, Study on the aging mechanism of boron potassium nitrate (B/KNO_3) for sustainable efficiency in pyrotechnic mechanical devices, Sci. Rep. 8 (2018) 11745.
[40] J. Oh, S. Jang, J.J. Yoh, Towards understanding the effects of heat and humidity on ageing of a NASA standard pyrotechnic igniter, Sci. Rep. 9 (2019) 10203.
[41] S. Sinha, N.W. Piekiel, G.L. Smith, C.J. Morris, Investigating aging effects for porous silicon energetic materials, Combust. Flame 181 (2017) 164–171.
[42] D.N. Sorensen, A.P. Quebral, E.E. Baroody, W.B. Sanborn, Investigation of the thermal degradation of the aged pyrotechnic titanium hydride/potassium perchlorate, J. Therm. Anal. Calorim. 85 (2006) 151–156.
[43] X. Zhao, X. Fu, G. Zhang, X. Liu, X. Fan, Study on the cocrystallization mechanism of CL-20/HMX in a propellant aging process through theoretical calculations and experiments, ACS Omega 7 (2022) 7361–7369.
[44] C.S. Gorzynski, J.N. Maycock, Explosives and pyrotechnic propellants for use in long term deep space missions, J. Spacecraft Rockets 11 (1974) 211–212.
[45] B.J. Bellott, W. Noh, R.G. Nuzzo, G.S. Girolami, Nanoenergetic materials: boron nanoparticles from the pyrolysis of decaborane and their functionalisation, Chem. Commun. 22 (2009) 3214–3215.
[46] H. Wang, M. Rehwoldt, D.J. Kline, T. Wu, P. Wang, M.R. Zachariah, Comparison study of the ignition and combustion characteristics of directly-written Al/PVDF, Al/Viton and Al/THV composites, Combust, Flame 201 (2019) 181–186.
[47] H. Wang, J.B. DeLisio, S. Holdren, T. Wu, Y. Yang, J. Hu, M.R. Zachariah, Mesoporous silica spheres incorporated aluminum/poly (vinylidene fluoride) for enhanced burning propellants, Adv. Eng. Mater. 20 (2017) 1700547.
[48] J.B. DeLisio, X. Hu, T. Wu, G.C. Egan, G. Young, M.R. Zachariah, Probing the reaction mechanism of aluminum/poly(vinylidenefluoride) composites, J. Phys. Chem. B 120 (2016) 5534–5542.
[49] W. Ao, J. Zhou, J. Liu, W. Yang, Y. Wang, H. Lia, Kinetic model of single boron particle ignition based upon both oxygen and (BO)n diffusion mechanism, Combust. Explos. Shock Waves 50 (2014) 262–271.
[50] D. Liang, J. Liu, Y. Zhou, J. Zhou, K. Cen, Ignition delay kinetic model of boron particle based on bidirectional diffusion mechanism, Aero. Sci. Technol. 73 (2018) 78–84.